The Numerical Simulation of Welding Residual Stress of Dissimilar Transparent Thermoplastics with MZA Powder Absorbent

Xiaodong Yu[1], Jie Zhang[3] and Chuanyang Wang[2,*]

[1]School of Mechanical Engineering, Suzhou University of Science and Technology, Suzhou, 215009, China

[2]School of Mechanical and Electrical Engineering, Soochow University, Suzhou, 215021, China

[3]Qingdao Air++ New Materials Co., Ltd., Qingdao, 266109, China

Abstracts: There are residual stresses in the joint caused by swift temperature variation in the process of laser transmission welding with metal absorbent. However, the related forming process is hard to detect through experimental methods. Herein, a physical model is established to describe the evolution of stress during the welding of polyarylsulfone (PASF) and polycarbonate (PC). The evolution of heat stress and the forming of residual stress is analyzed through the method of heat-force sequential coupling. In this process, the condensate transition, metal powder deformation, and clamping forces are involved in the mathematical model of stress-strain. In this model, the stress history can be divided into n time intervals according to the principle of superimposed stresses. The results revealed a significant correlation between the thermal history and stress evolution. Furthermore, the maximum von-mises stress appeared at the time of 1.7 s, then there was a decreasing tendency and stabled at 9 s. The von-mises stress was considered as residual stress after that time and the related stress distribution was investigated. The findings of this study provide a comprehensive understanding of residual stress on the joint.

Keywords: Numerical simulation, Residual stress, Laser transmission welding, Dissimilar thermoplastics, Metal powders.

INTRODUCTION

Thermoplastics have the advantages of reprocessing, low weight, high strength and excellent weathering resistance [1]. There is a great application in the files of aerospace [2], automotive [3], consumer electronics [4] and medical [5]. For examples, the fabrication of car headlights [6] and flexible sensors [7] ask for the connection of thermoplastics with properties of large size, specific properties, complex structure, and so on. The traditional forming technology, such as extrusion, injection and blow molding, cannot meet processing requirements [8]. It is urgent to generated a stable connection technology to overcome the shortcomings of traditional forming technology. As a result, the thermoplastics have a wider range of applications.

Comparing with mechanical connection and bonding technology, the welding technology presents numerous advantages in connecting thermoplastics. Because of the high efficiency, good stability and easy automation, the welding technology is commonly used for connecting of green and high value-added plastic products [6]. The welding technology is classified into ultrasonic welding, friction welding and induction welding, *et al*., because of the difference of heat source. Laser has the properties of high precision and good application, and can be used as heat source. The related technology is named as laser transmission welding (LTW). TLW creates a small heat-affected zone, is easy to automate and control, and does not contaminate [9].

As for the dissimilar transparent thermoplastics, there are shortcomings of incompatible and poor laser energy utilization, specific laser absorbents are necessary during the LTW process [10]. Chen *et al*. [11] proposed a cleaner production method for laser transmission welding of two transparent PMMA parts using multi-core copper wire. Besides, Wang *et al*. [12] and Liu *et al*. [13] claimed that the high thermal conductivity of the metal favors the advantages as a laser absorber. The recently research results show that the metal powders have ability of transferring light into heat and generating mechanical riveted structures in the joint [12, 14, 15]. However, there are obvious difference of thermos-physical properties between metal powders and thermoplastics. The internal stresses, forming during the welding process, leads to cracks and holes in joint. Those defects have negative effects on weld. It is urgent to analyze the evolution of stresses in the relevant processes.

Herein, the welding process of polyarylsulfone (PASF) and polycarbonate (PC) with magnesium-zinc alloy (MZA) powder absorbent is selected for research. A physical model of welding process is established, and the stress distribution and evolution are analyzed through superposition of transient temperature field and transient stress field. The research results are of great significance for understanding the stress evolution, optimizing the welding process and improving the welding quality.

*Address correspondence to this article at the School of Mechanical and Electrical Engineering, Soochow University, Suzhou, 215021, China;
Tel: 86-512-65790192; E-mail: cywang@suda.edu.cn

E-ISSN: 2410-4701/23 © 2023 Zeal Press

1. LASER TRANSMISSION WELDING

A well-established bonding strength depends on both a good fusion of molecular within the heat-affected zone and a low residual stress in the joint [16]. During the LTW process, the transparent thermoplastics components are aligned together by clamping pressure before the welding. As shown in Figure **1**, the laser beam passes through the upper transparent thermoplastics, and is absorbed by MZA powder absorbent. the generated heat contributes to the melt of thermoplastics. The entanglement of molecular chain creates a bond between the two transparent thermoplastics components when the temperature is greater than the melting point.

As for the welding process of PASF and PC with MZA powder absorbent, a three-dimensional symmetrical physical model for the thermal description of LTW is developed as shown in Figure **2**(**a**). The size of the model is 10 × 6 × 4 mm^3. The thickness of upper and lower thermoplastics is 2 mm. In order to simplify the calculation, the MZA powder absorbent layer is considered as a bulk film with the size of 10 × 1.5 × 0.08 mm^3. The simplified MZA bulk film is positioned between the upper and lower thermoplastics. The effects of node sensitivity on thermal response is investigated. We set five different minimum mesh size: 0.04 mm, 0.07 mm 0.1 mm, 0.13 mm, 0.16 mm. The simulated width of weld seam gradually stabilizes with the smaller meshing size and is consistent with the experimental width of joint. When the minimum meshing size is less than 0.1 mm, the simulation requires longer time. Therefore, in order to save computing time, the minimum meshing size in this paper was set as 0.1 mm. An adaptive hexahedral mesh is chosen for meshing, and the overall number of meshes is 35389. The mesh result with skewness of 0.88 is displayed in Figure **2**(**b**).

The time-dependent properties of PASF and PC are considered in the simulation. The parameters of thermoplastics and MZA powders used for numerical simulation is displayed in Table **1**, which are provided by the supplier. The spatial temperature field is verified based on the comparison between simulated and experimental joint morphology. Based on the thermal calculations, we developed a thermomechanical model for determining the residual stress distribution in the joint. The calculations of temperature distribution and

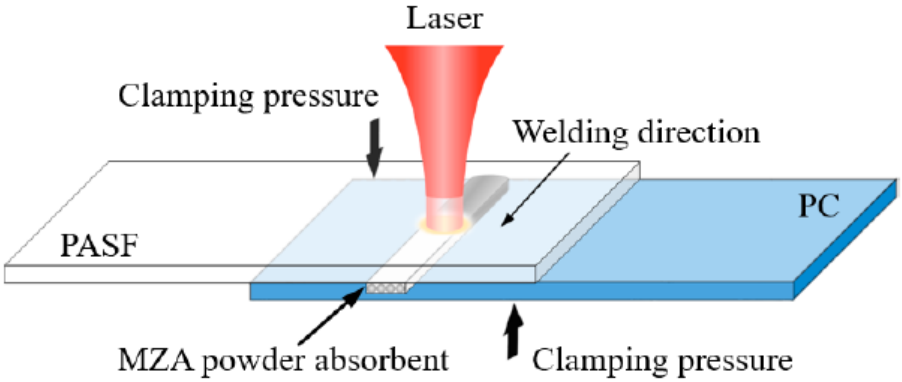

Figure 1: Schematic diagram of laser transmission welding.

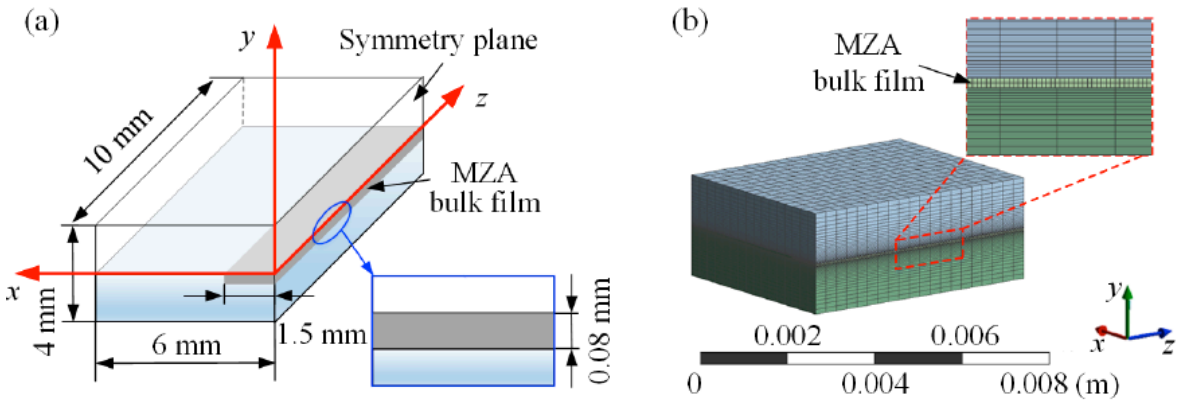

Figure 2: Physical modeling (**a**) and meshing results (**b**).

Table 1: The Physical Properties of PASF and PC

Property	PASF	PC	MZA powder
Young's modulus (MPa)	2550	2530	45000
Poisson's ratio	0.4	0.38	0.35
The shear modulus (MPa)	910.71	916.67	16667
Bulk modulus (MPa)	4250	3513.9	50000
Melting temperature (℃)	327.5	278.1	/
Coefficient of thermal expansion ($℃^{-1}$)	5.5×10^{-5}	6.8×10^{-5}	2.6×10^{-5}
Glass transition temperature (℃)	288	145	/
The heat distortion temperature (℃)	274	131	/
Density ($g\cdot cm^{-3}$)	$\rho=\begin{cases}1494.3, & 27℃\le T<327℃\\ 1397.9, & 327℃\le T\end{cases}$	$\rho=\begin{cases}-0.319T+1207, & 27℃\le T\le145℃\\ -0.685T+1253, & T>27℃\end{cases}$	/
Thermal conductivity ($W\ (m\cdot K)^{-1}$)	$k=(3\times10^{-4})T+0.201,\ T\ge27℃$	$k=\begin{cases}(2.493\times10^{-4})T+0.186, & 27℃\le T\le145℃\\ -(5.536\times10^{-5})T+0.23, & T>145℃\end{cases}$	/
Specific heat capacity ($J\cdot(kg\cdot K)^{-1}$)	$C=3.756T+1763,\ T\ge27℃$	$C=\begin{cases}3.42T+1120.67, & 27℃\le T<140℃\\ 27.385T-2236.38, & 140℃\le T<147℃\\ 1.771T+1537.41, & T\ge147℃\end{cases}$	/
Thermal decomposition temperature (℃)	487.4	402.3	/
Light transmittance (%)	87.39	88.53	/
Absorbance (abs)	0.05	0.07	/
Light reflectance (%)	10.72	4.2	/

residual stresses are conducted in sequential coupling. The specific flow chat of welding stress simulation is displayed as Figure **3**.

The aim of the subsequent investigation is therefore the relationship between welding temperature and residual stress. The related model assumptions and boundary conditions are shown as following.

(1) Materials are isotropic, including the PASF and PC composites.

(2) Symmetry strategy is adopted to shorten the simulation time.

(3) The contact between mating parts is perfect.

(4) The thermal evolution is considered and neglect the flow physics [17].

(5) The thermo-physics properties of materials are temperature independence [3].

3. THE MATHEMATICAL MODEL USED FOR THERMOMECHANICAL SIMULATION

3.1 The Heat Source Model

According to the first law of thermodynamics, the welding temperature is investigated by numerical simulation [18]. The governing equation for energy transfer is as Equation (1).

$$\rho\cdot c(T)\cdot\frac{\partial T}{\partial z}=\nabla\cdot(\lambda(T)\cdot\nabla T)+\Phi \quad (1)$$

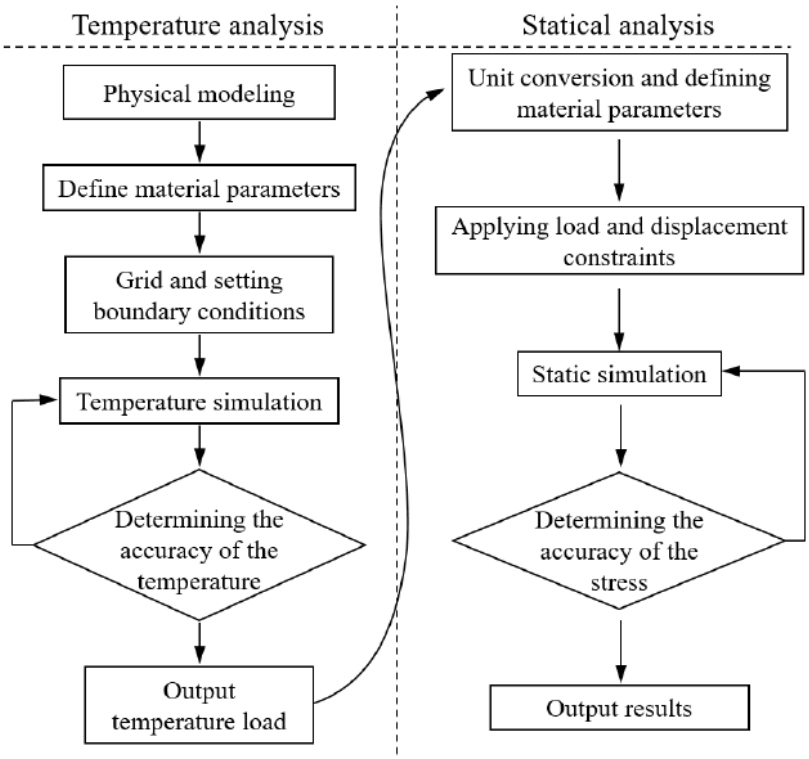

Figure 3: The specific flow chat of welding stress simulation.

Where T ($^{\circ}C$) is the temperature, c (J/(kg$^{\circ}C$)) is the specific heat capacity, λ (W/(m$^{\circ}C$)) is the thermal conductivity, ∇ is the gradient scattering. The laser energy flux distribution (Φ) along the radial direction is defined in Equation (2).

$$\Phi=\left|\frac{\partial I_{(r,t)}}{\partial r}\right| \tag{2}$$

The pure PASF and PC is laser-transparent at the wavelength of 980 nm. The MZA powder could improve the absorptivity. It is demonstrated that high thermal conductivity of metal materials contributes to the heat transferring, the type of heat distribution tends to be volume. Herein, the mathematical model of volume heat source ($I(r,t)$) generated by laser-MZA powder interaction is described as Equation (3) [19].

$$I_{(x,y,z,t)}=\frac{6\cdot P\cdot\eta}{\left(\left(z-vt\right)^2+\left(x\right)^2\right)\cdot u_y} \tag{3}$$

Where P (W) is the laser power, v (m/s) is the laser moving velocity, η is correction coefficient, u_y (m) is the depth of laser action zone.

3.2 The Material Constitutive Equation for Thermo Mechanical Calculation

The analysis of welding stress-strain field is the solution of nonlinear transient problem, which contains material nonlinearity and geometric nonlinearity. The solution process is based on the elastic-plastic mechanics model, with the incremental theory of calculation, according to the principle of strain superposition, the material's intrinsic equation is expressed as Equation (4).

$$d\varepsilon_{ij} = d\varepsilon_{ij}^{E} + d\varepsilon_{ij}^{P} + d\varepsilon_{ij}^{T} \tag{4}$$

Where ε_{ij}^{E} is the elastic strain tensor, ε_{ij}^{P} is the plastic strain tensor, ε_{ij}^{T} is the thermal strain tensor.

According to the Hooke's law, the elastic strain tensor is expressed as Equation (5).

$$d\varepsilon_{ij}^{E} = \frac{1}{E_T}\left[\left(1+\upsilon\right)d\sigma_{ij} - \upsilon d\sigma_{ij}\delta_{ij}\right] \tag{5}$$

Where E_T is the material elasticity modulus, σ_{ij} is the stress increment, υ is the poisson's ratio, δ_{ij} is the unit matrix

The plastic strain tensor is described by Prandtl-Reuss plastic flow theory as Equation (6) [20]:

$$\begin{cases} d\varepsilon_{ij}^{P} = 0,\ \Phi<0 \ \text{ or } \ \dfrac{\partial\Phi}{\partial\sigma_{ij}}d\sigma_{ij}\leqslant 0 \\ d\varepsilon_{ij}^{P} = \dfrac{3}{2H'}\dfrac{d\bar{\sigma}}{\bar{\sigma}}\dfrac{\partial\Phi}{\partial\sigma_{ij}},\ \Phi=0 \ \text{ or } \ \dfrac{\partial\Phi}{\partial\sigma_{ij}}d\sigma_{ij}>0 \end{cases} \tag{6}$$

Where Φ is the yield surface, $\bar{\sigma}$ is the equivalent force, H' is the tangential modulus.

The thermal strain tensor caused by temperature gradient is expressed as Equation (7).

$$d\varepsilon_{ij}^{T} = \alpha_T \cdot dT \cdot \delta_{ij} \tag{7}$$

Where α_T ($^{\circ}C^{-1}$) is the coefficient of thermal expansion at specific temperature.

When the weld is finished, the weld temperature decreased from maximum value (T_t) to the room temperature (T_0). There is assuming that the coefficient of thermal expansion of the material is isotropic, the materials strain increment $\Delta\varepsilon_{cool}$ is expressed as Equation (8) [21].

$$\Delta\varepsilon_{cool} = \left(\alpha_1(T) - \alpha_2(T)\right)\Delta T \tag{8}$$

Where $\alpha_1(T)$ and $\alpha_2(T)$ is the coefficient of thermal expansion of MZA powder and thermoplastics, respectively.

Furthermore, the heat-generated strain in metal powders is considered. The related shrinkage stress σ_{cool} in the cool process is expressed as Equation (9) [22].

$$\sigma_{cool} = \int_{T_t}^{T_0} \left(E_1(T)\alpha_1(T) - E_2(T)\alpha_2(T) \right) dT \tag{9}$$

Where $E_1(T)$ and $E_2(T)$ is the modulus of elasticity of MZA powder and thermoplastics, respectively.

Considering the effect of shrinkage stress and clamping force during cooling, the stress state of the welded joint can be expressed as follow.

$$\begin{aligned} \sigma_r^{T_0} &= \sigma_r - \sigma_{cool} \\ \sigma_\theta^{T_0} &= \sigma_\theta - \sigma_{cool} \end{aligned} \tag{10}$$

where $\sigma_r^{T_0}$ and $\sigma_\theta^{T_0}$ is the longitudinal and transverse stresses in welded joints at room temperature.

4. RESULTS AND DISCUSSION

4.1. The Evolution of Welding Temperature

In the case of joint morphology, Casalino *et al*. [23] divided the weld into three parts: the core zone, the melt zone and the heat affected zone (HAZ), as shown in Figure **4**(**a**). It is clearly that the simulated and experimental core zone is on the MZA powder layer. The related temperature is 345 $^{\circ}C$. The core zone is surrounded by the melt zone, and followed by HAZ. The boundary of HAZ is related to the heat distortion temperature of PASF with 274 $^{\circ}C$ and PC with 131 $^{\circ}C$. It can be concluded that the simulated and experimental boundary of HAZ is overlap.

The curve of weld temperature is recorded as Figure **4**(**b**), when the laser line energy is 5 J/mm. The welding temperature has an increasing tendency in the welding process (0 s ~ 1.6 s). The maximum temperature of 345 $^{\circ}C$ appears at 1.7 s. This is due to that there is a hysteresis of temperature during the heat transfer according to Long *et al*. [24]. Mostly, the heat transfers through conduction and convection to the surroundings. When the time is 1.7 s, the laser moved to the end. The loss of energy reduced at this time and resulted in high temperature. After welding, the temperature decreases to 142 $^{\circ}C$ at the time of 2.7 s. the temperature is below the glass transition temperature of both PASF with 288 $^{\circ}C$ and PC with 145 $^{\circ}C$. A stable joint forms after this time.

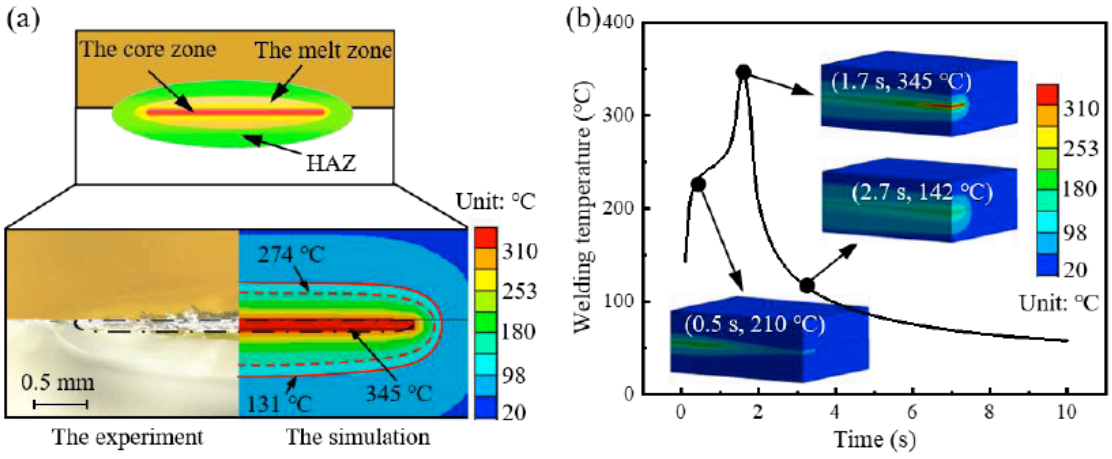

Figure 4: The experimental and simulated joint morphology (**a**) and the variation of welding temperature with time (**b**).

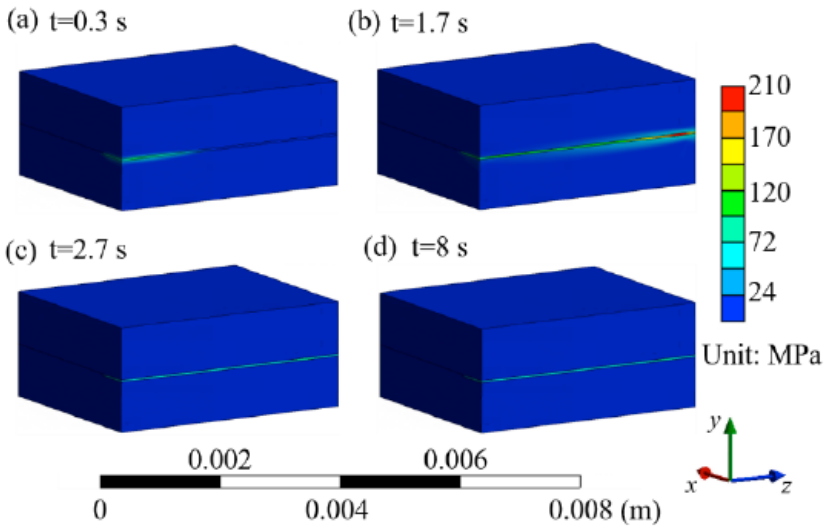

Figure 5: The cloud maps of von-mises stress at different time.

4.2. The Evolution of Thermal Stress

The thermoplastics melts with laser radiation, and then volume expansion occurs. Limited by the surrounding material, compressive stress forms at this time. Because of the uneven temperature distribution during welding, the internal constriction is also uneven. The welding stresses and distortion can be attributed to the different degrees of internal constriction [21]. After cooling, the molecular chains orient along the direction of internal constriction, and then the internal stresses form because that molecular chains have tendency of reverting to their original state. According to Mohr's strength theory, von-mises stress is used to determine the plastic yielding. As shown in Figure **5**, the maximum von-mises stress appears at the laser spot, and moving with the laser when the time is from 0 s to 1.7 s. After welding (Figure **5**(**c**)), the von-mises stress decreases and centers on MZA layer. Combining with the temperature results, the joint fully cures when the time is 2.7 s. After that, there are no significant differences on the cloud maps of Figure **5**(**d**).

The curve of von-mises stress as function of time is displayed in Figure **6**. During the welding process, the von-mises stress has a slight decreasing trend. This is due to the good thermal conductivity of MZA layer contributes to a uniform distribution of welding temperature. When the laser moves to the end (t=1.7 s), the von-mises stress increases sharply to the maximum value (about 193.8 MPa). There is a high agreement between the evolution of the welding temperature curve and the von-mises stress curve. Sudden increase of temperature leads to large temperature gradients, so there is a sudden increase of von-mises stress. After welding, the von-mises stress decreases rapidly and tends to stabilize when the time is over 9 s. The von-mises stress is defined as residual stress after this point.

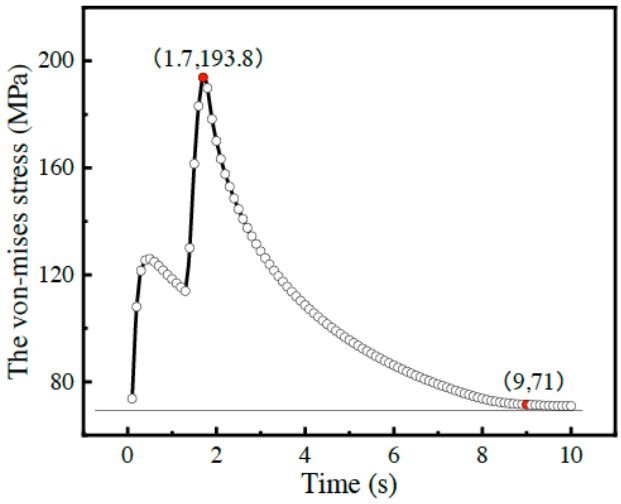

Figure 6: The curve of von-mises stress as function of time.

4.3. The Distribution of Residual Stress

The transverse residual stress is perpendicular to the weld as shown in Figure **7**(**a**). Normally, there are two different forms of residual stress distribution along paths of I-I and II-II, respectively. On the path of I-I, parallel to the direction of the weld, the transverse residual stress is tensile according to Figure **7**(**b**). This is due to the fact that the contraction and deformation of the weld is limited by the surrounding material during the cooling process, thus forming the tensile effect. And the distribution of the residual stress has the characteristic of "saddle-like", and the residual stresses are larger at the beginning and the end positions of the weld. This is similar to the evolution of the von-mises stress in the welding process. On the path of II-II,

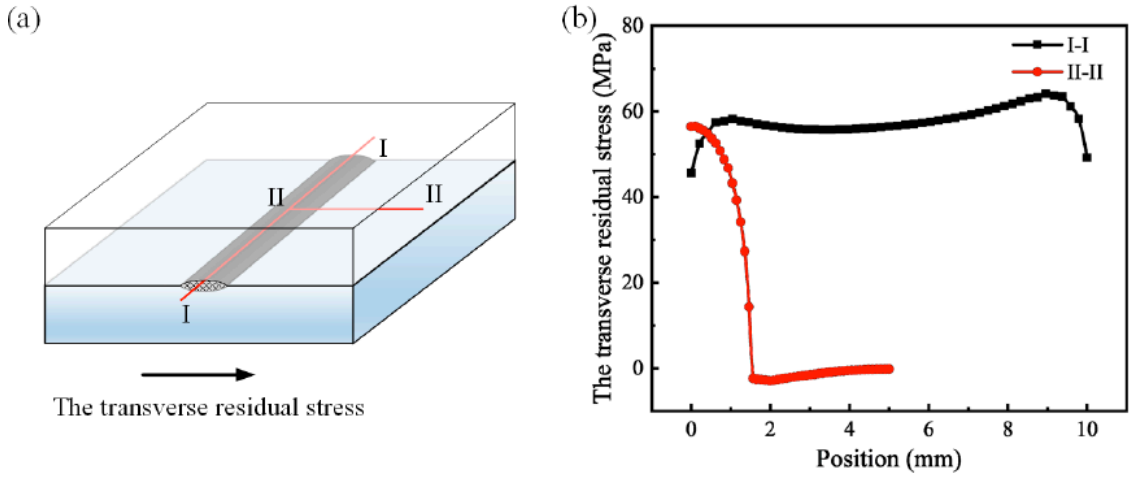

Figure 7: The transverse residual stress: schematic diagram of selected positions (**a**), distribution of residual stress (**b**).

perpendicular to the direction of the weld, it is clear that the residual stress within the compressive plastic deformation zone around the weld (0 ~ 1.5 mm) behave as tensile, and within the transition zone away from the weld (> 1.5 mm) behave as compressive. Only half of the stress distribution is shown according to the curve of II-II, this is because there is an axisymmetric setup during the simulation

The transverse residual stress is in the direction perpendicular to the weld as shown in Figure **8**(**a**). The black line in Fig. 8(b) shows the longitudinal residual stresses in the path (I-I) parallel to the weld direction. The longitudinal residual stresses are tensile and also have a "saddle-like" character. However, the longitudinal residual stresses at the ends of the weld tend to be close to 0. This is due to the lack of material constraints at the start and end points of the weld, which are free in the longitudinal direction. The red line in Figure **8**(**b**) shows the longitudinal residual stresses on the path (II-II) perpendicular to the weld. There are larger residual compressive stresses in the transition region away from the weld (>1.5 mm), which are due to the fact that there is a significant solid-liquid transition in the transition region of the weld. The temperature gradients contribute to the formation of inhomogeneous plastic deformations and consequently to larger residual compressive stresses.

The thickness residual stress is in the direction of the sample thickness as shown in Figure **9**(**a**). The distribution of thickness residual stress along the trails of O-O is displayed in Figure **9**(**b**). It is clear that the residual stress in the thickness direction is tensile and centers on the MZA powder layer. There is a significant tensile-compressive residual stress transitions in the region where the MZA powder layer is in excess of the plastic matrix.

5. CONCLUSION

As for the laser transmission welding of PASF and PC with MZA powder absorbent, the simulated results indicate that the variation of von-miss stress is closely

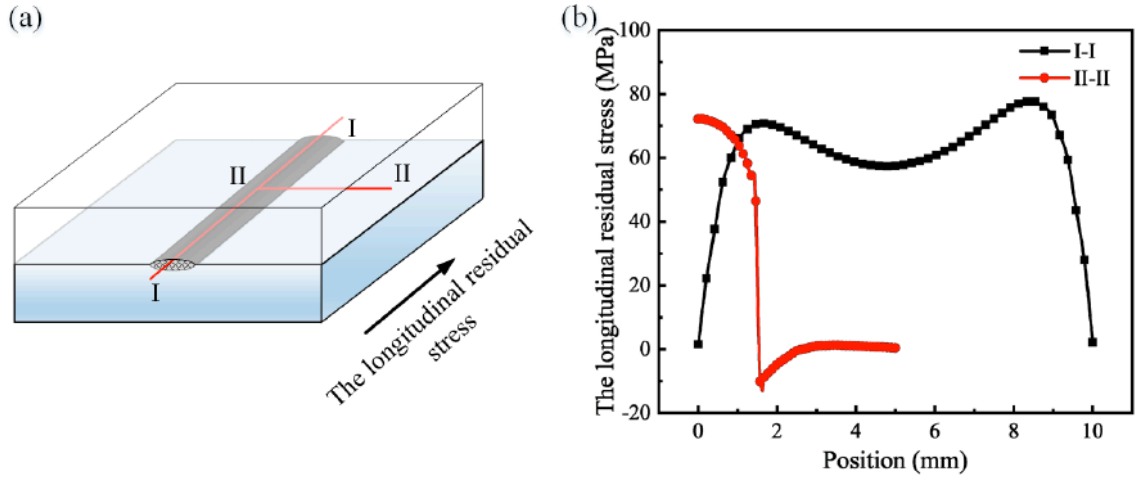

Figure 8: The longitudinal residual stress: schematic diagram of selected positions (**a**), distribution of residual stress (**b**).

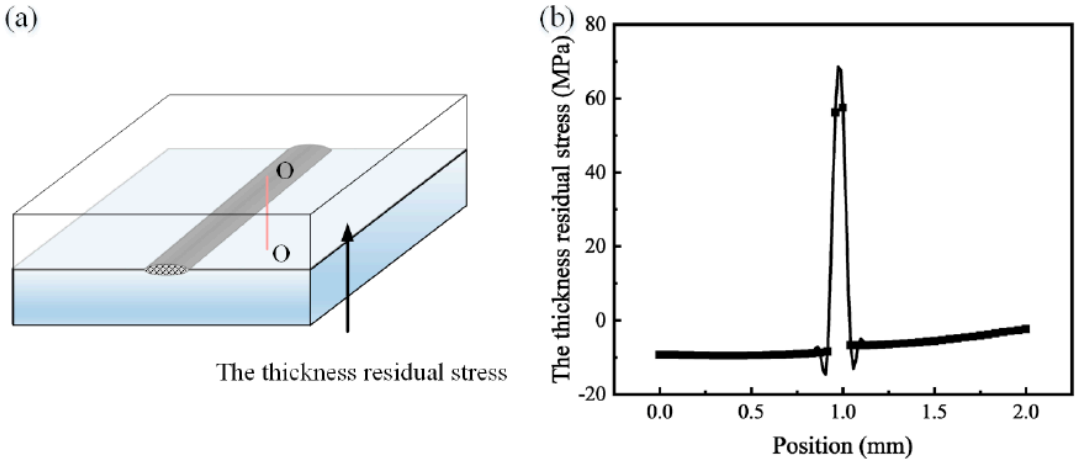

Figure 9: The thickness residual stresses: schematic diagram of selected locations (**a**), distribution of residual stresses (**b**)

related to the temperature distribution. Both of maximum temperature and von-mises appear at time of 1.7 s. And then there is rapidly decreasing process. The transverse residual stress parallel to the weld direction is dominated by tensile stress and the related stress distribution is characterized by "saddle-like". There is a significant tensile-compressive stress transition in the path perpendicular to the weld direction. The thickness residual stress is concentrated in the MZA powder layer.

DISCLOSURE STATEMENT

No potential conflict of interest was reported by the author(s).

FUNDING

This work is supported by the National Natural Science Foundation of China (No. 52075354), the fellowship of China Postdoctoral Science Foundation (No. 2020M681699).

REFERENCES

[1] G. Zhang, J. Qiu, Ultrasonic thermal welding of immiscible thermoplastics via the third phase, Journal of Materials Processing Technology 299 (2022) 117330. https://doi.org/10.1016/j.jmatprotec.2021.117330

[2] A. Costa, E.C. Botelho, M.L. Costa, N.E. Narita, J.R. Tarpani, A Review of Welding Technologies for Thermoplastic Composites in Aerospace Applications, Journal of Aerospace Technology Management 4(3) (2012) 255-265. https://doi.org/10.5028/jatm.2012.040303912

[3] X. Wang, B. Liu, W. Liu, X. Zhong, Y. Jiang, H. Liu, Investigation on the Mechanism and Failure Mode of Laser Transmission Spot Welding Using PMMA Material for the Automotive Industry, Materials (Basel) 10(1) (2017) 22. https://doi.org/10.3390/ma10010022

[4] H. Becker, C. Gartner, Polymer microfabrication technologies for microfluidic systems, Anal. Bioanal. Chem. 390(1) (2008) 89-111. https://doi.org/10.1007/s00216-007-1692-2

[5] T. Velten, H.H. Ruf, D. Barrow, N. Aspragathos, P. Lazarou, J. Erik, C.K. Malek, M. Richter, J. Kruckow, M. Wackerle, Packaging of bio-MEMS: strategies, technologies, and applications, IEEE Transactions on Advanced Packaging 28(4) (2005) 533-546. https://doi.org/10.1109/TADVP.2005.858427

[6] B. Acherjee, Laser transmission welding of polymers – A review on welding parameters, quality attributes, process monitoring, and applications, Journal of Manufacturing Processes 64 (2021) 421-443. https://doi.org/10.1016/j.jmapro.2021.01.022

[7] B. Acherjee, Laser transmission welding of polymers – A review on process fundamentals, material attributes, weldability, and welding techniques, Journal of Manufacturing Processes 60 (2020) 227-246. https://doi.org/10.1016/j.jmapro.2020.10.017

[8] P. Groche, S. Wohletz, M. Brenneis, C. Pabst, F. Resch, Joining by forming—A review on joint mechanisms, applications and future trends, Journal of Materials Processing Technology 214(10) (2014) 1972-1994. https://doi.org/10.1016/j.jmatprotec.2013.12.022

[9] A. Gisario, F. Veniali, M. Barletta, V. Tagliaferri, S. Vesco, Laser transmission welding of poly(ethylene terephthalate) and biodegradable poly(ethylene terephthalate) - Based blends, Optics and Lasers in Engineering 90 (2017) 110-118. https://doi.org/10.1016/j.optlaseng.2016.10.010

[10] A. Gisario, M. Mehrpouya, E. Pizzi, Dissimilar joining of transparent Poly(ethylene terephthalate) to aluminum 7075 sheets using a diode laser, Journal of Laser Applications 29(2) (2017). https://doi.org/10.2351/1.4983268

[11] Z. Chen, H. Zhou, C. Wu, F. Han, H. Yan, A cleaner production method for laser transmission welding of two transparent PMMA parts using multi-core copper wire, Journal of Materials Research and Technology 16 (2022) 1-12. https://doi.org/10.1016/j.jmrt.2021.11.157

[12] C. Wang, X. Yu, M. Jiang, Fracture forms and multiple undulated morphology of polycarbonate LTW by introducing carbon black coated copper film, Optics and Laser Technology 141 (2021). https://doi.org/10.1016/j.optlastec.2021.107132

[13] M. Liu, D. Ouyang, J. Zhao, C. Li, H. Sun, S. Ruan, Clear plastic transmission laser welding using a metal absorber, Optics & Laser Technology 105 (2018) 242-248. https://doi.org/10.1016/j.optlastec.2018.02.047

[14] Yu Xiaodong, Jiang Muhui, Zhang Gongda, Wang Chuanyang, Influences of Copper Film Width on Polycarbonate Welding Strength and Welding Morpholog, AcOpS 41(14) (2021). https://doi.org/10.3788/AOS202141.1414001

[15] X.D. Yu, H.Y. Qiao, Z.Y. Chen, Y. Chen, Q. Li, Y. Liu, C. Wang, Mechanism and factor analysis of welding PC and PASF using magnesium zinc alloy particles as laser-absorbent, Optics & Laser Technology 158 (2023)

108859.
https://doi.org/10.1016/j.optlastec.2022.108859

[16] A. Yousefpour, M. Hojjati, J.P. Immarigeon, Fusion Bonding/Welding of Thermoplastic Composites, Journal of Thermoplastic Composite Materials 17(4) (2004) 303-341.
https://doi.org/10.1177/0892705704045187

[17] C. Hopmann, S. Bölle, S. Kreimeier, Modeling of the thermally induced residual stresses during laser transmission welding of thermoplastics, Welding in the World 63(5) (2019) 1417-1429.
https://doi.org/10.1007/s40194-019-00770-9

[18] M. Van Elsen, M. Baelmans, P. Mercelis, J.P. Kruth, Solutions for modelling moving heat sources in a semi-infinite medium and applications to laser material processing, International Journal of Heat and Mass Transfer 50(23-24) (2007) 4872-4882.
https://doi.org/10.1016/j.ijheatmasstransfer.2007.02.044

[19] X. Yu, H. Qiao, Y. Chen, Q. Li, Z. Chen, Y. Liu, C. Wang, An integrated methodology for estimating the interface temperature and effects of powder diameters in laser transmission welding process, Science and Technology of Welding and Joining 28(7) (2023) 589-597.
https://doi.org/10.1080/13621718.2023.2187543

[20] Y. Ai, K. Zheng, Y.C. Shin, B. Wu, Analysis of weld geometry and liquid flow in laser transmission welding between polyethylene terephthalate (PET) and Ti6Al4V based on numerical simulation, Optics & Laser Technology 103 (2018) 99-108.
https://doi.org/10.1016/j.optlastec.2018.01.022

[21] P.P. Parlevliet, H.E.N. Bersee, A. Beukers, Residual stresses in thermoplastic composites—A study of the literature—Part I: Formation of residual stresses, Composites Part A: Applied Science and Manufacturing 37(11) (2006) 1847-1857.
https://doi.org/10.1016/j.compositesa.2005.12.025

[22] D. Bonefeld, V. Schoppner, H. Potente, R. Mahnken, A. Shaban, Residual Stresses in the Quasi-Simultaneous Laser Transmission Welding of Amorphous Thermoplastics, Polymer Engineering and Science 50(8) (2010) 1520-1526.
https://doi.org/10.1002/pen.21685

[23] E. Ghorbel, G. Casalino, S. Abed, Laser diode transmission welding of polypropylene: Geometrical and microstructure characterisation of weld, Materials & Design 30(7) (2009) 2745-2751.
https://doi.org/10.1016/j.matdes.2008.10.027

[24] Q. Long, H. Qiao, X. Yu, Y. Liu, C. Wang, Modeling and experiments of the thermal degradation behavior of PMMA during laser transmission welding process, International Journal of Heat and Mass Transfer 194 (2022) 123086.
https://doi.org/10.1016/j.ijheatmasstransfer.2022.123086

Received on 18-11-2023 Accepted on 15-12-2023 Published on 20-12-2023

DOI: https://doi.org/10.31875/2410-4701.2023.10.12

© 2023 Yu *et al.*; Zeal Press.
This is an open access article licensed under the terms of the Creative Commons Attribution License (http://creativecommons.org/licenses/by/4.0/) which permits unrestricted use, distribution and reproduction in any medium, provided the work is properly cited.